Electronic Supplementary Information

Experimental section

Materials: Sodium nitrite ($NaNO_2$, 99.9%), ammonium chloride (NH_4Cl, 99.5%), sodium hydroxide (NaOH, 98%), ethanol (C_2H_6O, 99.9%), sodium salicylate ($C_7H_5NaO_3$, 99.5%), trisodium citrate dihydrate ($C_6H_5Na_3O_7 \cdot 2H_2O$, 99%), p-dimethylaminobenzaldehyde ($C_9H_{11}NO$, 99%), sodium nitroferricyanide dihydrate ($C_5FeN_6Na_2O \cdot 2H_2O$, 99%) and sodium hypochlorite solution (NaClO, 5%) were purchased from Aladdin Co., Ltd. (Shanghai, China). Sulfuric acid (H_2SO_4, 99%), hydrogen peroxide (H_2O_2, 99%), hydrochloric acid (HCl, 99%), hydrazine monohydrate ($N_2H_4 \cdot H_2O$, 99%) and ethyl alcohol (C_2H_5OH, 99%) were bought from Beijing Chemical Corporation. (China). Ti plate (thickness is 0.2 mm, 99.9%) was purchased from Qingyuan Metal Materials Co., Ltd (Xingtai, China). All reagents used in this work were analytical grade without further purification.

Preparation of TiO_2 nanosheets array: Firstly, Ti plate (2.0 × 3.0 cm^2) was cleaned by ultrasonication in acetone, ethanol, and water for 15 min, respectively. Then, Ti plate was put into a 50 mL of Teflon-lined autoclave containing 35 mL of 5 M NaOH solution and heated in an electric oven at 180 °C for 24 h. Subsequently, cation exchange of Na^+ to H^+ was carried out by immersing the sample into 1 M HCl for 1 h to obtain $H_2Ti_2O_5 \cdot H_2O$ nanosheet array, followed by annealing at 500 °C for 2 h.

Preparation of CoB@TiO_2 nanoarray: Amorphous CoB was magnetron sputtered onto as-prepared TiO_2 nanoarray. The sputtering chamber was evacuated to about 8×10^{-4} Pa before the sputtering deposition. Ar (50 sccm) was injected to the chamber with a total pressure of 4 Pa and the sputtering voltage was 310 V (direct current voltage). The bias voltage was 60 V and the sputtering time was 5 min. CoB on Ti plate was prepared by the same procedure. The sputtering machine (Z/CM GXZ 05-2020) is purchased from Chengdu CM Photoelectrictechnology Co., Ltd.

Characterizations: XRD data were acquired from a LabX XRD-6100 X-ray diffractometer with a Cu Kα radiation (40 kV, 30 mA) of wavelength 0.154 nm

(SHIMADZU, Japan). SEM images were collected on a Gemini SEM 300 scanning electron microscope (ZEISS, Germany) at an accelerating voltage of 5 kV. TEM images were acquired on a HITACHI H-8100 electron microscopy (Hitachi, Tokyo, Japan) operated at 200 kV. XPS measurements were performed on an ESCALABMK II X-ray photoelectron spectrometer using Mg as the exciting source. The absorbance data of spectrophotometer was measured on UV-vis spectrophotometer (SHIMADZU UV-2700). Gaseous products from nitrate reduction reaction were determined by gas chromatography (GC) with SHIMADZU GC-2014 gas chromatograph.

Electrochemical measurements: All electrochemical measurements were carried out on the CHI660E electrochemical workstation (Chenhua, Shanghai). A three-electrode system with an H-type electrolytic cell separated by a Nafion 117 membrane, working electrode of a piece of CoB@TiO_2/TP as, reference electrode of Ag/AgCl, and counter electrode of graphite rod are used for the electrochemical tests under magnetic stirring (250 rpm). Electrolyte is 0.1 M Na_2SO_4 with/without 400 ppm NO_2^-. The potentials reported in this work were converted to the reversible hydrogen electrode (RHE) via the equation of E (vs. RHE) = E (vs. Ag/AgCl) + 0.197 V + 0.059 × pH.

Determination of NH_3: NH_3 concentration was spectrophotometrically determined by the indophenol blue method (the obtained electrolyte was diluted 20 times). In detail, 4 mL diluted electrolyte was mixed with 50 μL oxidizing solution containing NaClO (4.5%) and NaOH (0.75 M), 500 μL coloring solution containing $C_7H_5O_3Na$ (0.4 M) and NaOH (0.32 M), and 50 μL 1 wt% $Na_2Fe(CN)_5NO{\cdot}2H_2O$ aqueous solution for 1 h in darkness. The concentration-absorbance curve (y = 0.4506x + 0.0238, R^2 = 0.9998) was prepared from the UV-vis spectra of the standard NH_4Cl solutions with known concentrations of 0, 1, 2, 3, 4 mL^{-1} in 0.1 M Na_2SO_4.

Determination of N_2H_4: N_2H_4 was estimated by the Watt and Chrisp method. The color reagent was a solution of 18.15 mg mL^{-1} of $C_9H_{11}NO$ in the mixed solvent of HCl and C_2H_5OH (V/V: 1/10). In detail, 2 mL electrolyte was added into 2 mL color reagent for 15 min under stirring. The absorbance of such solution was measured to

quantify the hydrazine yields by the standard curve of hydrazine (y = 0.6878x + 0.1066, R^2 = 0.9998).

Determination of N_2, H_2: H_2 was quantified by GC.

Calculations of the m_{NH3}, FE and NH_3 yield:

The amount of NH_3 (m_{NH3}) was calculated by the following equation:

$$m_{NH3} = [NH_3] \times V$$

FE of NH_3 formation was calculated by the following equation:

$$FE = (6 \times F \times [NH_3] \times V) / (M_{NH3} \times Q) \times 100\%$$

NH_3 yield rate is calculated using the following equation:

$$NH_3 \text{ yield} = ([NH_3] \times V) / (M_{NH3} \times t \times A)$$

Where F is the Faradic constant (96485 C mol^{-1}), $[NH_3]$ is the NH_3 concentration, V is the volume of electrolyte in the anode compartment (40 mL), M_{NH3} is the molar mass of NH_3 molecule, Q is the total quantity of applied electricity, t is the electrolysis time (1 h) and A is the geometric area of working electrode (0.5 × 0.5 cm^2).

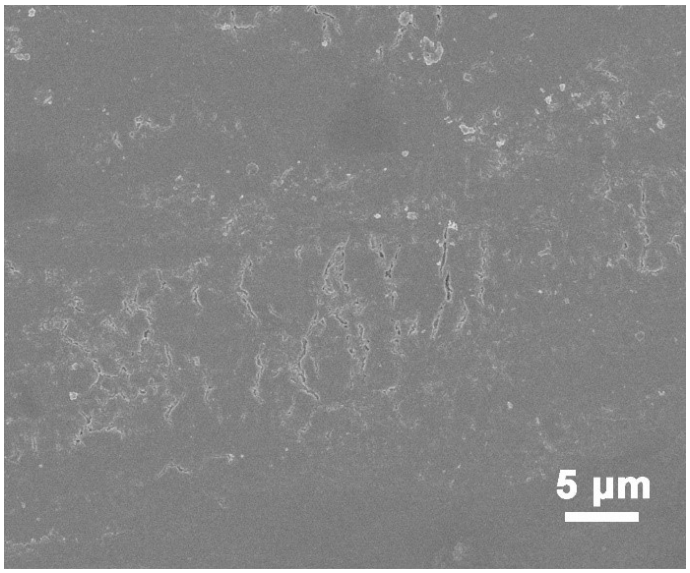

Fig. S1. SEM image of TP.

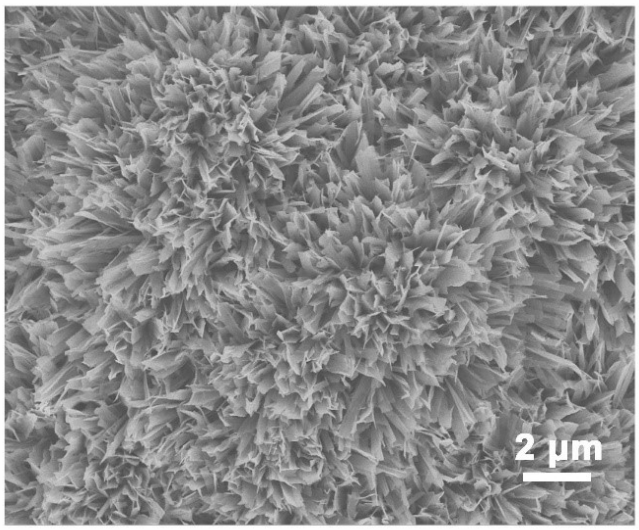

Fig. S2. SEM image of TiO_2/TP.

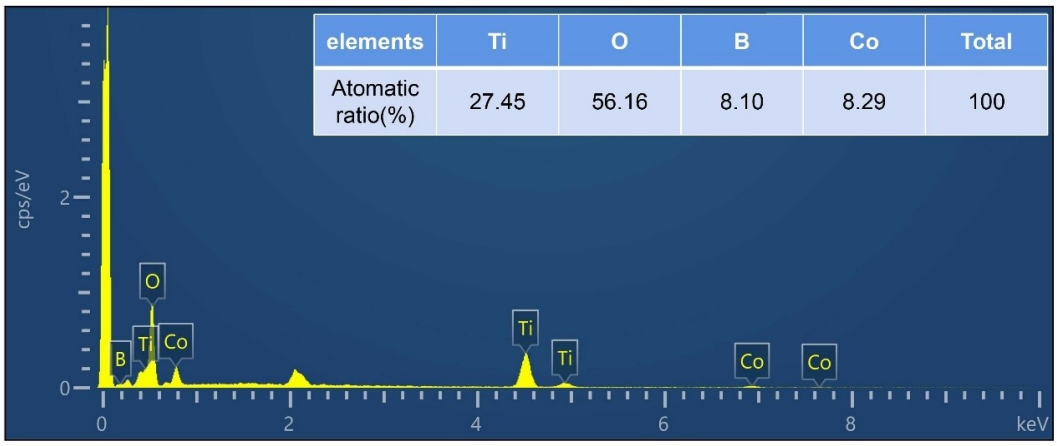

Fig. S3. EDX spectrum of $CoB@TiO_2/TP$.

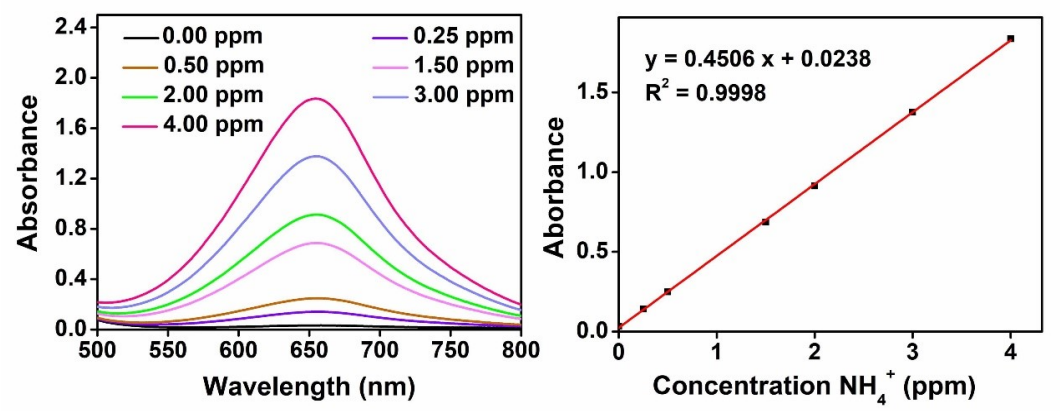

Fig. S4. (a) UV-vis spectra and (b) corresponding calibration curve for calculation of NH_4^+ concentration.

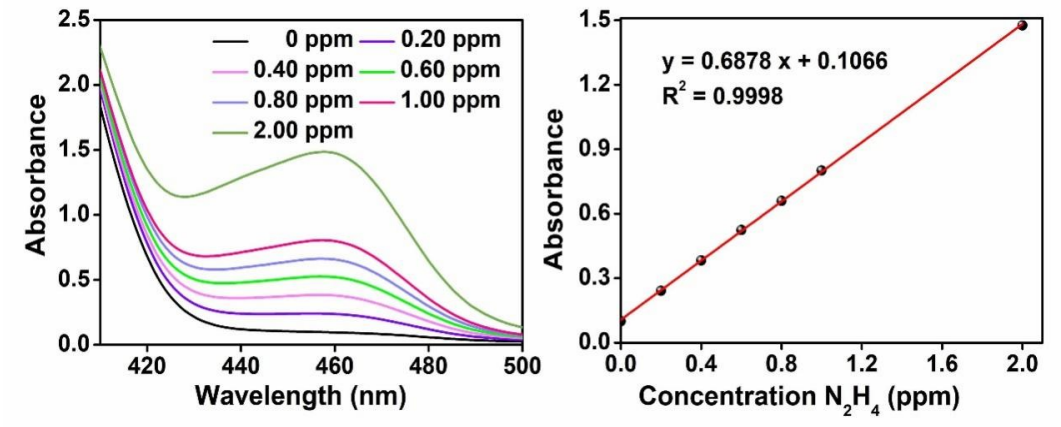

Fig. S5. (a) UV-vis spectra and (b) corresponding calibration curve for calculation of N_2H_4 concentration.

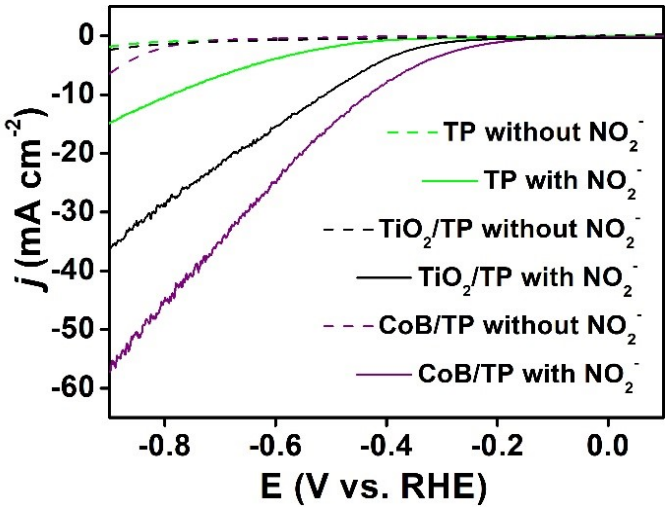

Fig. S6. LSV curves of CoB/TP, TiO_2/TP, and bare TP in 0.1 M Na_2SO_4 with/without 400 ppm NO_2^-.

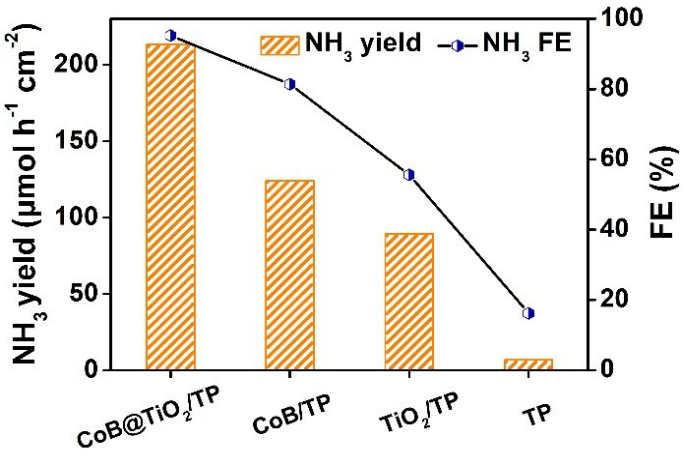

Fig. S7. NH_3 yields and FEs of CoB@TiO_2/TP, CoB/TP, TiO_2/TP, and bare TP in 0.1 M Na_2SO_4 containing 400 ppm NO_2^- at −0.7 V.

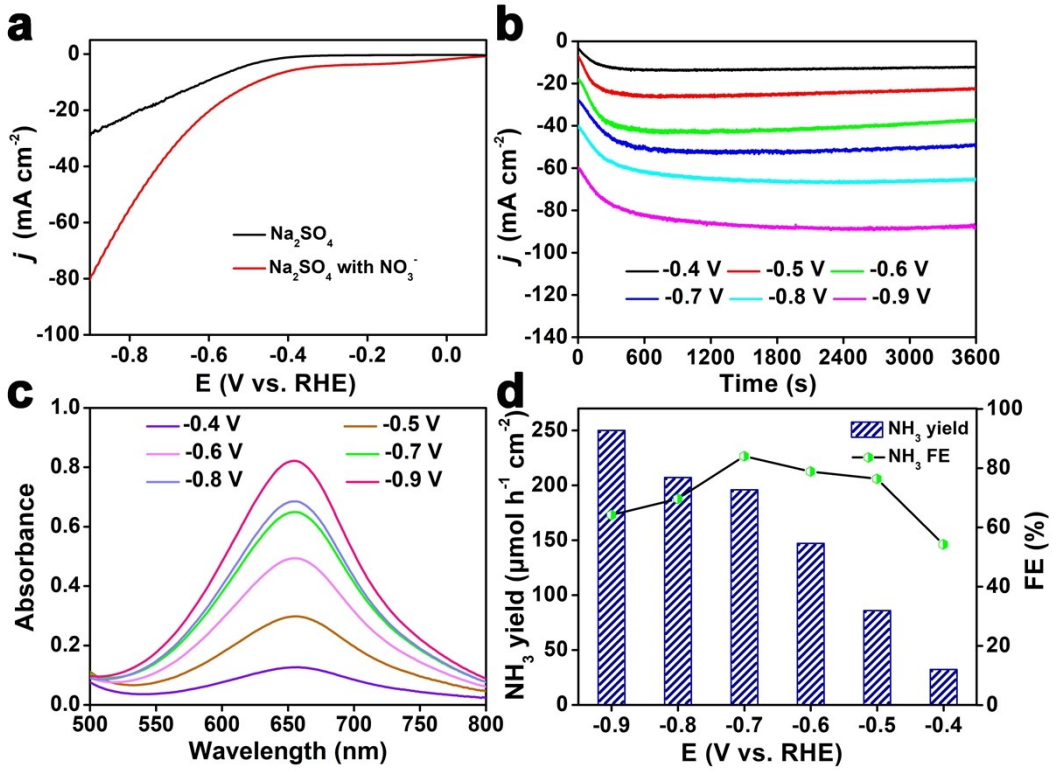

Fig. S8. NO_3^- reduction reaction performance measurements of CoB@TiO_2/TP: (a) LSV curves in 0.1 M Na_2SO_4 with and without 400 ppm NO_3^-. (b) Chronoamperometry curves and (c) corresponding UV-vis spectra at a potential rang from −0.4 V to −0.9 V. (d) NH_3 yields and FEs at given potentials.

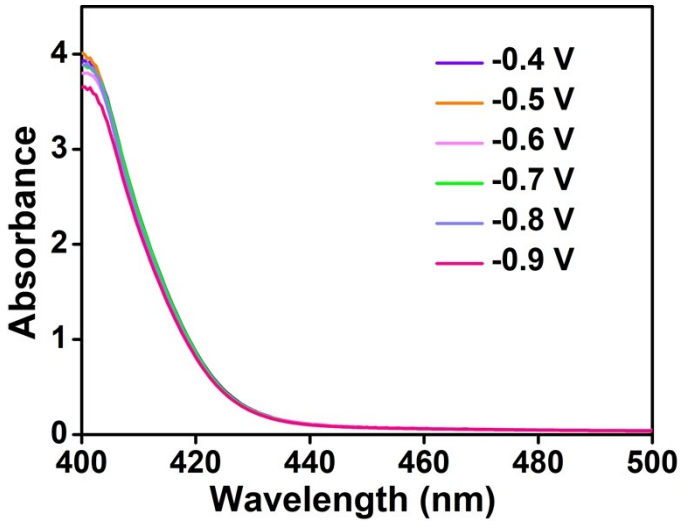

Fig. S9. UV-vis spectra of N_2H_4 detection.

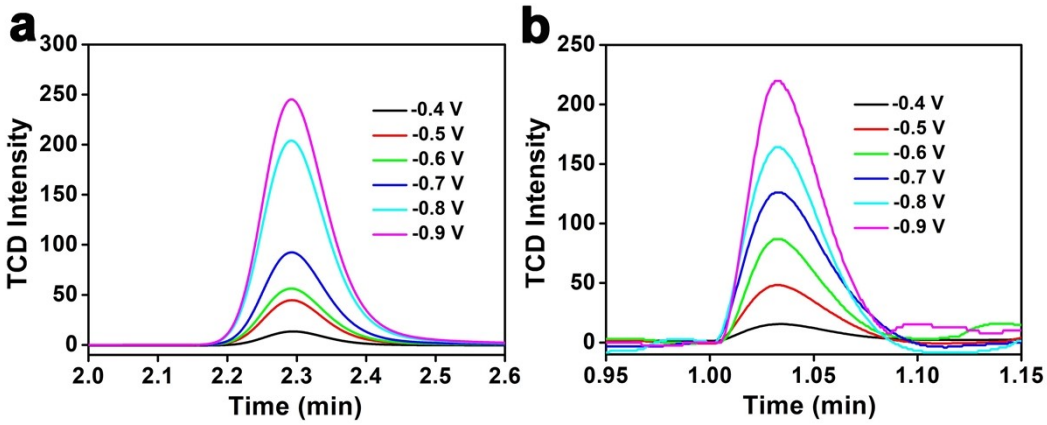

Fig. S10. Chromatograph curves of (a) H_2 and (b) N_2 detected by GC at each given potential.

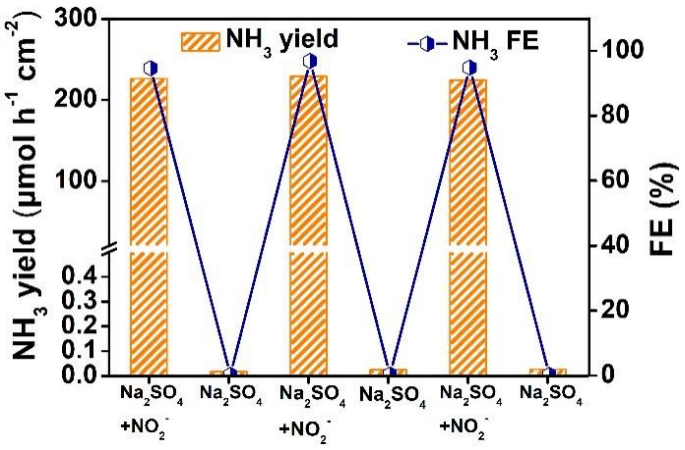

Fig. S11. NH_3 yields and FEs during alternating cycle tests between NO_2^--containing and NO_2^--free 0.1 M Na_2SO_4 at −0.7 V.

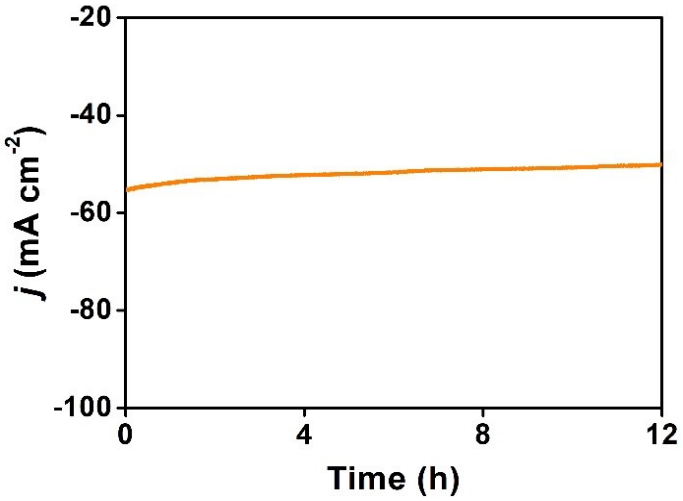

Fig. S12. Chronoamperometry curve of CoB@TiO_2/TP during 12-h stability test.

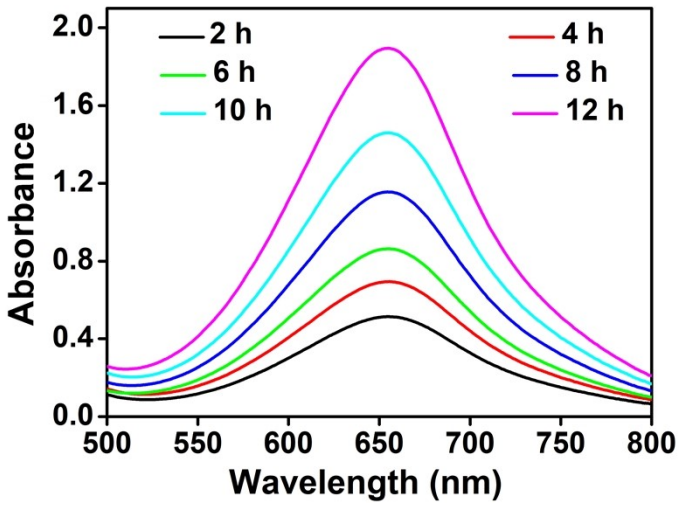

Fig. S13. Time-dependent UV-vis spectra of NH_4^+ during long-term stability test.

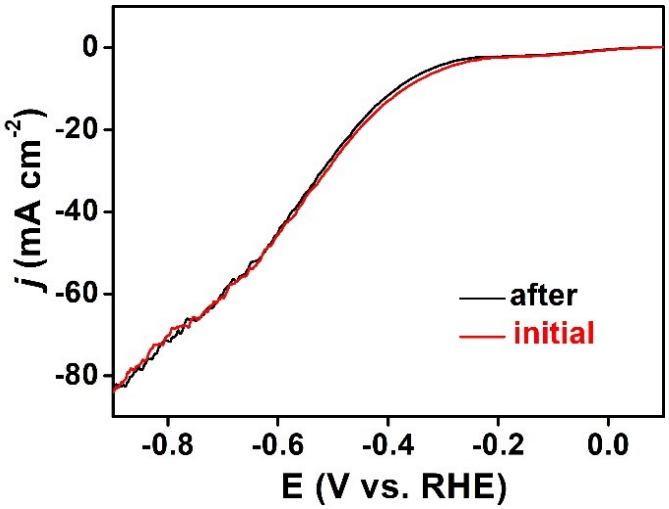

Fig. S14. LSV curves of CoB@TiO_2/TP before and after long-term stability test.

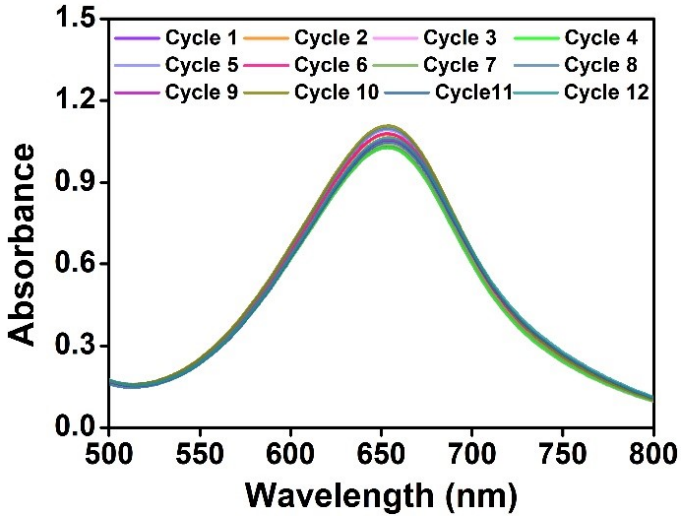

Fig. S15. UV-vis spectra of CoB@TiO_2/TP for cycling tests in 0.1 M Na_2SO_4 containing 400 ppm NO_2^- at −0.7 V.

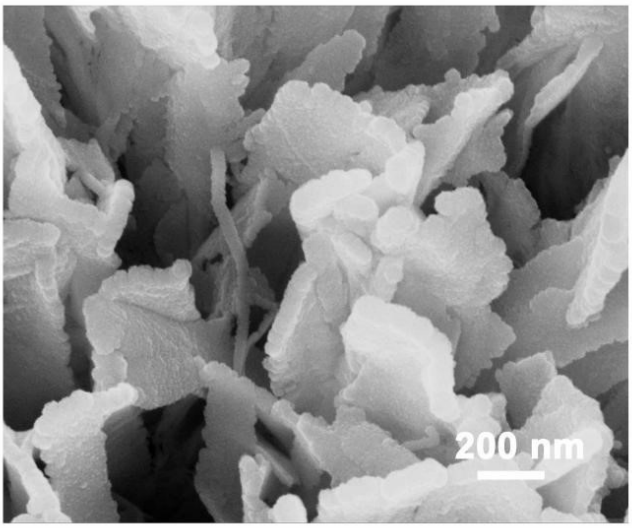

Fig. S16. SEM image of CoB@TiO_2/TP after durability test.

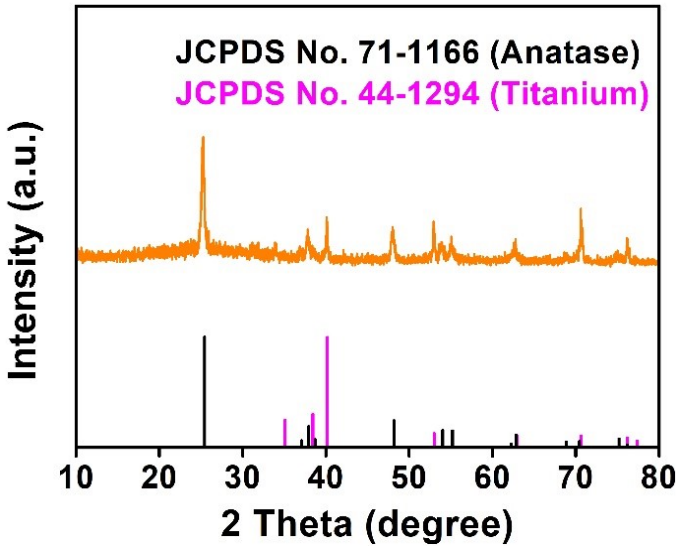

Fig. S17. XRD pattern of CoB@TiO_2/TP after durability test.

Table S1. Comparison of the catalytic performances of CoB@TiO_2/TP with the other reported NO_2^-RR and NO_3^-RR electrocatalysts.

Catalyst	Electrolyte	NH_3 yield	FE (%)	Ref.
CoB@TiO_2/TP	0.1 M Na_2SO_4 (400 ppm $NaNO_2$)	233.1 μmol h^{-1} cm^{-2}	95.2	This work
	0.1 M Na_2SO_4 (400 ppm $NaNO_3$)	195.9 μmol h^{-1} cm^{-2}	84	
MnO_2 nanoarray	0.1 M Na_2SO_4 (0.2 M $NaNO_2$)	8.6×10^{-12} μmol h^{-1} cm^{-2}	6	1
Ni-NSA-V_{Ni}	0.2 M Na_2SO_4 (200 ppm $NaNO_2$)	235.5 μmol h^{-1} cm^{-2}	88.9	2
Cobalt-tripeptide complex	1.0 M MOPS (1.0 M $NaNO_2$)	1.1 μmol h^{-1} cm^{-2}	90 ± 3	3
Ni_2P/NF	0.1 M PBS (200 ppm $NaNO_2$)	158.1 ± 5.4 μmol h^{-1} cm^{-2}	90.2 ± 3.0	4
CoP NA/TM	0.1 M PBS (500 ppm $NaNO_2$)	132.7 ± 3.0 μmol h^{-1} cm^{-2}	90.0 ± 2.3	5
Cu_3P NA/CF	0.1 M PBS (0.1 M $NaNO_2$)	95.5 ± 2.1 μmol h^{-1} cm^{-2}	91.2 ± 2.5	6
$Cu_{80}Ni_{20}$	1.0 M NaOH (20 mM $NaNO_2$)	/	87.6	7
Cu phthalocyanine complexes	0.1 M KOH ($NaNO_2$)	/	78	8
$[Co(DIM)Br_2]^+$	0.1 M $NaNO_2$	/	88	9
FeN_5H_2	1.0 M MOPS	/	18	10
Co_3O_4@NiO	0.5 M Na_2SO_4 (2.36 mM $NaNO_3$)	/	55.0	11

Co/CoO NSA	0.1 M Na_2SO_4 (200 ppm $NaNO_3$)	194.5 μmol h^{-1} cm^{-2}	93.8	12
Co_2AlO_4	0.1 M PBS (0.1 M $NaNO_3$)	464.7 μmol h^{-1} cm^{-2}	92.6	13
Pd nanodots on Zr-MOF	0.1 M Na_2SO_4 (500 ppm NO_3^-)	16.99 μmol h^{-1} $mg_{cat.}^{-1}$	58.1	14
Ru_xO_y clusters on Ni-MOF	0.1 M Na_2SO_4 (100 ppm NO_3^-)	16.1 μmol h^{-1} $mg_{cat.}^{-1}$	58.8	15
Fe single atom catalyst	0.10 M K_2SO_4 (0.50 M KNO_3)	~1176 μmol h^{-1} cm^{-2}	~75	16
Ag@NiO/CC	0.1 M NaOH (0.1 M $NaNO_3$)	135.1 μmol h^{-1} cm^{-2}	75.8	17

References

1 R. Wang, Z. Wang, X. Xiang, R. Zhang, X. Shi and X. Sun, MnO_2 nanoarrays: an efficient catalyst electrode for nitrite electroreduction toward sensing and NH_3 synthesis applications, *Chem. Commun.*, 2018, **54**, 10340–10342.

2 C. Wang, W. Zhou, Z. Sun, Y. Wang, B. Zhang and Y. Yu, Integrated selective nitrite reduction to ammonia with tetrahydroisoquinoline semi-dehydrogenation over a vacancy-rich Ni bifunctional electrode, *J. Mater. Chem. A*, 2021, **9**, 239–243.

3 Y. Guo, J. R. Stroka, B. Kandemir, C. E. Dickerson and K. L. Bren, Cobalt metallopeptide electrocatalyst for the selective reduction of nitrite to ammonium, *J. Am. Chem. Soc.*, 2018, **140**, 16888–16892.

4 G. Wen, J. Liang, L. Zhang, T. Li, Q. Liu, X. An, X. Shi, Y. Liu, S. Gao, A. M. Asiri, Y. Luo, Q. Kong and X. Sun, Ni_2P nanosheet array for high-efficiency electrohydrogenation of nitrite to ammonia at ambient conditions, *J. Colloid Interface Sci.*, 2022, **606**, 1055–1063.

5 G. Wen, J. Liang, Q. Liu, T. Li, X. An, F. Zhang, A. A. Alshehri, K. A. Alzahrani, Y. Luo, Q. Kong and X. Sun, Ambient ammonia production via electrocatalytic nitrite reduction catalyzed by a CoP nanoarray, *Nano Res.*, 2022, **15**, 972–977.

6 J. Liang, B. Deng, Q. Liu, G. Wen, Q. Liu, T. Li, Y. Luo, A. A. Alshehri, K. A. Alzahrani, D. Ma and X. Sun, High-efficiency electrochemical nitrite reduction to ammonium using a Cu_3P nanowire array under ambient conditions, *Green Chem.*, 2021, **23**, 5487–5493.

7 L. Mattarozzi, S. Cattarin, N. Comisso, P. Guerriero, M. Musiani, L. Vázquez-Gómez and E. Verlato, Electrochemical reduction of nitrate and nitrite in alkaline media at CuNi alloy electrodes, *Electrochim. Acta*, 2013, **89**, 488–496.

8 N. Chebotareva and T. Nyokong, Metallophthalocyanine catalysed electroreduction of nitrate and nitrite ions in alkaline media, *J. Appl. Electrochem.*,

1997, **27**, 975–981.

9 S. Xu, H.-Y. Kwon, D. C. Ashley, C.-H. Chen, E. Jakubikova and J. M. Smith, Intramolecular hydrogen bonding facilitates electrocatalytic reduction of nitrite in aqueous solutions, *Inorg. Chem.*, 2019, **58**, 9443–9451.

10 J. R. Stroka, B. Kandemir, E. M. Matson and K. L. Bren, Electrocatalytic multielectron nitrite reduction in water by an iron complex, *ACS Catal.*, 2020, **10**, 13968–13972.

11 Y. Wang, C. Liu, B. Zhang and Y. Yu, Self-template synthesis of hierarchically structured Co_3O_4@NiO bifunctional electrodes for selective nitrate reduction and tetrahydroisoquinolines semi-dehydrogenation. *Sci. China Mater.*, 2020, **63**, 2530–2538.

12 Y. Yu, C. Wang, Y. Yu, Y. Wang and B. Zhang, Promoting selective electroreduction of nitrates to ammonia over electron-deficient Co modulated by rectifying schottky contacts. *Sci. China Chem.*, 2020, **63**, 1469–1476.

13 Z. Deng, J. Liang, Q. Liu, C. Ma, L. Xie, L. Yue, Y. Ren, T. Li, Y. Luo, N. Li, B. Tang, A. A. Alshehri, I. Shakir, P. O. Agboola, S. Yan, B. Zheng, J. Du, Q. Kong and X. Sun, High-efficiency ammonia electrosynthesis on self-supported Co_2AlO_4 nanoarray in neutral media by selective reduction of nitrate. *Chem. Eng. J.*, 2022, **435**, 135104.

14 M. Jiang, J. Su, X. Song, P. Zhang, M. Zhu, L. Qin, Z. Tie, J.-L. Zuo and Z. Jin, Interfacial reduction nucleation of noble metal nanodots on redox-active metal–organic frameworks for high-efficiency electrocatalytic conversion of nitrate to ammonia, *Nano Lett.* 2022, **22**, 2529–2537.

15 J. Qin, K. Wu, L. Chen, X. Wang, Q. Zhao, B. Liu and Z. Ye, Achieving high selectivity for nitrate electrochemical reduction to ammonia over MOF-supported Ru_xO_y clusters, *J. Mater. Chem. A* 2022, **10**, 3963-3969.

16 Z.-Y. Wu, M. Karamad, X. Yong, Q. Huang, D. A. Cullen, P. Zhu, C. Xia, Q. Xiao, M. Shakouri, F.-Y. Chen, J. Y. Kim, Y. Xia, K. Heck, Y. Hu, M. S. Wong

,Q. Li, I. Gates, S. Siahrostami and H. Wang, Electrochemical ammonia synthesis via nitrate reduction on Fe single atom catalyst, *Nat. Commun.* 2021, **12**, 2870.

17 Q. Liu, G. Wen, D. Zhao, L. Xie, S. Sun, L. Zhang, Y. Luo, A. A. Alshehri, M. S. Hamdy, Q. Kong and X. Sun, Nitrite reduction over Ag nanoarray electrocatalyst for ammonia synthesis, *J. Colloid Interface Sci.* 2022, **623**, 513–519.